Progress In Electromagnetics Research C, Vol. 78, 145–158, 2017

The Role of Hybrid Modes in Extraordinary Optical Transmission through a Plasmonic Nanohole Array

Christopher Trampel*

Abstract—A mode-matching solution to plane wave scattering by a plasmonic nanohole array consisting of a silver film perforated by an infinite square array of circular holes is presented. A complete orthonormal basis set consisting of waveguide modes satisfying an impedance boundary condition on the hole wall is derived. Impedance boundary conditions are satisfied on the upper and lower horizontal surfaces of the film and on the walls of the hole. Extraordinary optical transmission (EOT) is studied over optical wavelengths. Theory predicts a peak transmission value that is in better agreement with experiment than previous modal studies. The effect of film thickness on coupling between modes bound to the upper and lower surfaces is studied. The transmission profile for thinner films evinces two peaks at different wavelengths resulting from strong coupling between surface waves bound to the upper and lower surfaces. For thicker films, the surface waves decouple and a single peak is observed. The effect of hole radius on EOT is considered. It is demonstrated that transmission peaks occur for holes of a roughly constant electrical size. A relationship between the lattice constant and the transmission-to-area efficiency is quantified.

1. INTRODUCTION

Structured noble metals have been the subject of much interest in recent years due to their potential as nanophotonic devices [1]. A number of useful optical and plasmonic properties of such metals have been observed [2–6]. Plasmonic nanostructures exhibit properties that differ from bulk geometries due to electron confinement [7]. Nanometallic objects are able to trap incident radiation, focusing it into very small volumes. Gold nanoparticles have been used to concentrate electromagnetic fields to increase Raman scattering in a molecular identification technique known as surface-enhanced Raman spectroscopy (SERS) [8]. Nanoparticles may be used to control membrane processes via thermoplasmonics [9, 10]. Nanostars have been used in cancer imaging based on surface-enhanced resonance Raman scattering (SERRS) [11]. Krenn et al. [12] report enhancement of over 600% in a chain of nanometer scale gold particles. The ability to confine light on very small scales circumvents a fundamental limitation of dielectric waveguides. In order for a mode to propagate along a waveguide with a dielectric core, the diameter of the core must be greater than half a wavelength in the core medium $d_{core} \geq \lambda_0/(2n_{core})$, the so-called diffraction limit. Here d_{core} is the core diameter, λ_0 the free space wavelength, and n_{core} the refractive index of the core. Due to the fact that their permittivity is negative at optical frequencies, conservation of momentum dictates that noble metals be able to support guided modes for smaller core diameters. Several plasmonic waveguide geometries have been proposed, including nanowires [13] and stripes [14]. Maier et al. demonstrate local energy transport along a waveguide consisting of silver rods [15]. As the losses in the metal limit propagation length, metal-insulator-metal (MIM) waveguides have also been studied [16]. Such waveguides typically consist of a dielectric layer sandwiched between two metal stripes. In MIM waveguides, coupling between

Received 30 May 2017, Accepted 30 September 2017, Scheduled 8 October 2017
* Corresponding author: Christopher Trampel (ctrampel@weber.edu).
The author is with the Department of Engineering, Weber State University, Ogden, UT 84408, USA.

surface plasmon polaritons on opposite metal surfaces confines the mode to the dielectric region where resistive losses are smaller.

This article focuses on electromagnetic scattering from a silver film perforated by a periodic array of circular holes (Figure 1). Such plasmonic nanohole arrays have been used extensively as biosensors [17, 18]. The frequency at which a plasmon supported by the nanoaperture array is excited is very sensitive to the refractive index of the surrounding material. Thus, plasmon frequency shifts may be used to detect the presence of an analyte binding to the surface of the biosensor [19]. Nanohole arrays have been intensely studied since the discovery that they allow much greater optical transmission [20] than single holes [21]. Much experimental and theoretical effort has been focused on understanding this extraordinary optical transmission (EOT). Numerical studies of periodic hole arrays have been made using the finite-difference time-domain (FDTD) method. Baida and Van Labeke study zero-order transmission efficiency through a gold film as a function of incident wavelength [22]. They demonstrate that transmission efficiency can be improved by replacing the holes with an array of annular apertures. Similar structures have been studied in the frequency-domain via scattering matrix methods [23]. Biswas et al. leverage the scattering matrix approach to study a subwavelength triangular lattice of holes in a platinum film coupled to a silicon photonic crystal [24]. Their model predicts a resonant absorption of incident radiation over infrared frequencies.

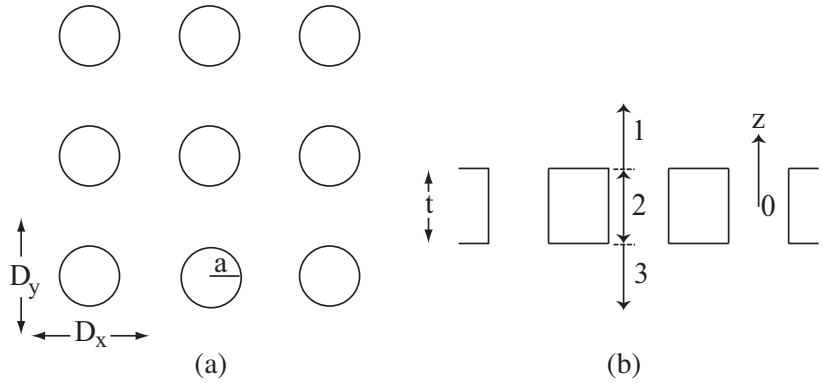

Figure 1. (a) Top and (b) side-view of silver film perforated by an infinite array of circular holes. The region above the film is designated 1, inside the hole 2, and below the film 3.

Martin-Moreno and Garcia-Vidal have studied scattering by a subwavelength square lattice of circular holes in a silver film via mode-matching [25]. Their approach may be summarized as follows. Above and below the film, the fields are expanded in terms of TM and TE Floquet harmonics. Waveguide modes are used inside the hole where the walls are treated as a perfect electric conductor (PEC). The unknown coefficients are found by enforcing boundary conditions at the upper and lower surfaces of the film. While the silver is treated as a PEC in [25], it is replaced with an impedance boundary condition (IBC) on the top and bottom surfaces of the film in [26]. The walls of the hole remain perfectly conducting, however. Zhang et al. [27] conduct a similar theoretical study of EOT through an array of circular holes. In their approach, the waveguide modes are determined by assuming an exponentially decaying field outside the hole rather than imposing an impedance boundary condition on the wall. While this approach is exact for an isolated hole, the assumption that the field in the metal can be modeled by a Hankel function with an imaginary argument may be problematic for a periodic geometry. Their approach agrees well with experimental data with respect to the position of transmission peaks and nulls. However, no quantitative measure of the error in the peak amplitudes is given. Impedance boundary conditions were also used to analyze transmission through an array of rectangular holes [28]. The assumption of an impedance boundary condition on the hole wall yields excellent quantitative results. Both the position and amplitude of the transmission peaks agree well with experiment.

This article extends the formalism in [26] to include an IBC on the walls of the hole. The addition of an impedance boundary condition on the hole walls is a significant improvement as it allows for a finite

tangential electric field on the wall surface. It also avoids the necessity to phenomenologically enlarge the holes to capture penetration into the metal [29]. The results herein predict a peak transmission that is much closer to the experimental value than that presented in [26]. While previous mode-matching studies predict similar qualitative results, the theory presented here permits accurate quantitative study of the EOT phenomenon. In addition, this approach avoids any explicit assumptions regarding the form of the solution in the metal region. The article is organized as follows. Section 2 introduces the scalar decomposition used to split the fields into TE and TM components. Section 3 details the derivation of the waveguide modes in the hole region with an impedance boundary condition on the walls. The modal expansions above and below the film and in the hole region are discussed in Section 4. A set of matrix equations for the unknown coefficients is solved in Section 5. Section 6 includes a discussion of the results, while our conclusions are collected in Section 7.

2. SCALAR DECOMPOSITION

For a preferred direction along the z-axis, the frequency-domain electric and magnetic fields may be written in terms of transverse magnetic (TM) and transverse electric (TE) scalar potentials thus [30]

$$\overline{E} = \nabla \times \nabla \times [\hat{\overline{z}}\psi] + \imath\omega\mu_p \nabla \times [\hat{\overline{z}}\varphi] \tag{1}$$

$$\overline{H} = -\imath\omega\epsilon_p \nabla \times [\hat{\overline{z}}\psi] + \nabla \times \nabla \times [\hat{\overline{z}}\varphi]. \tag{2}$$

Here ω is the frequency and ϵ_p, μ_p are respectively the permittivity and permeability of region p. Cylindrical coordinates are employed inside the hole. In cylindrical coordinates, the components of the electric and magnetic fields are

$$E_z = \left(\frac{\partial^2}{\partial z^2} + k_p^2\right)\psi \tag{3}$$

$$E_\rho = \frac{\partial^2 \psi}{\partial \rho \partial z} + \imath\omega\mu_p \frac{1}{\rho}\frac{\partial \varphi}{\partial \phi} \tag{4}$$

$$E_\phi = \frac{1}{\rho}\frac{\partial^2 \psi}{\partial \phi \partial z} - \imath\omega\mu_p \frac{\partial \varphi}{\partial \rho} \tag{5}$$

$$H_z = \left(\frac{\partial^2}{\partial z^2} + k_p^2\right)\varphi \tag{6}$$

$$H_\rho = -\imath\omega\epsilon_p \frac{1}{\rho}\frac{\partial \psi}{\partial \phi} + \frac{\partial^2 \varphi}{\partial \rho \partial z} \tag{7}$$

$$H_\phi = \imath\omega\epsilon_p \frac{\partial \psi}{\partial \rho} + \frac{1}{\rho}\frac{\partial^2 \varphi}{\partial \phi \partial z} \tag{8}$$

where $k_p^2 = \omega^2 \epsilon_p \mu_p$. Above and below the film, the scalar potentials and fields are expressed in Cartesian coordinates

$$E_x = \frac{\partial^2 \psi}{\partial x \partial z} + \imath\omega\mu_p \frac{\partial \varphi}{\partial y} \tag{9}$$

$$E_y = \frac{\partial^2 \psi}{\partial y \partial z} - \imath\omega\mu_p \frac{\partial \varphi}{\partial x} \tag{10}$$

$$E_z = \left(\frac{\partial^2}{\partial^2 z} + k_p^2\right)\psi \tag{11}$$

$$H_x = \frac{\partial^2 \varphi}{\partial x \partial z} - \imath\omega\epsilon_p \frac{\partial \psi}{\partial y} \tag{12}$$

$$H_y = \frac{\partial^2 \varphi}{\partial y \partial z} + \imath\omega\epsilon_p \frac{\partial \psi}{\partial x} \tag{13}$$

$$H_z = \left(\frac{\partial^2}{\partial^2 z} + k_p^2\right)\varphi. \tag{14}$$

The strategy for finding the potentials is as follows. Above and below the film, the Bloch-Floquet theorem guarantees a complete discrete basis set consisting of TE and TM Floquet modes [31]. Inside the hole, I expand the fields in terms of waveguide modes derived by imposing an impedance boundary condition on the hole wall. For azimuthal numbers other than zero, these waveguide modes involve coupled TE and TM potentials. As the hole region is radially finite, the waveguide modes are also a complete discrete basis [32]. The unknown coefficients are determined by enforcing boundary conditions on the upper and lower horizontal interfaces over a single unit cell.

3. WAVEGUIDE MODES

First I must determine the eigenmodes of the hole region while imposing an impedance boundary condition on the walls. I begin by writing the TM and TE potentials as Fourier series

$$\psi_h(\rho,\phi,z) = \sum_{n=-\infty}^{\infty} a_n \mathrm{J}_n(\gamma\rho)\exp(\imath n\phi)\exp(\imath\beta z) \tag{15}$$

$$\varphi_h(\rho,\phi,z) = \sum_{n=-\infty}^{\infty} b_n \mathrm{J}_n(\gamma\rho)\exp(\imath n\phi)\exp(\imath\beta z) \tag{16}$$

where $\mathrm{J}_n(\gamma\rho)$ is the Bessel function of the first kind, n an integer, β the axial wavenumber, $\gamma^2 = k^2 - \beta^2$, and a_n and b_n are unknown coefficients. On the walls of the hole I impose the following impedance boundary condition

$$\overline{E}_{tan} = Z\hat{\overline{n}} \times \overline{H} \tag{17}$$

where $\hat{\overline{n}}$ is a unit vector normal to the surface, and $Z = \sqrt{\mu_m/\epsilon_m}$ is the surface impedance of the metal. In this case $\hat{\overline{n}} = -\hat{\boldsymbol{\rho}}$. I employ the Drude free electron model [33] for the silver permittivity

$$\epsilon_{mr} = 1 - \frac{\omega_p^2}{(\omega^2 + \imath\gamma_p\omega)} \tag{18}$$

where γ_p is a damping coefficient, and the plasma frequency $\omega_p = 2\pi(8980)\sqrt{n_e}$ depends on the electron number density n_e. Here the damping coefficient $\gamma_p = 9\times10^{13}$ and the plasma frequency $\omega_p = 1.37\times10^{16}$. The IBC Eq. (17) leads to two equations

$$E_z(a) = -ZH_\phi(a) \tag{19}$$

and

$$E_\phi(a) = ZH_z(a). \tag{20}$$

Substituting Eqs. (15) and (16) into Eqs. (19) and (20) and exploiting orthogonality yields

$$\left[\gamma^2\mathrm{J}_n(\gamma a) + \imath Z\omega\epsilon\gamma\mathrm{J}'_n(\gamma a)\right] a_n - Z\beta n/a\mathrm{J}_n(\gamma a)b_n = 0 \tag{21}$$

and

$$\beta n/a\mathrm{J}_n(\gamma a)a_n + \left[\imath\omega\mu\gamma\mathrm{J}'_n(\gamma a) + Z\gamma^2\mathrm{J}_n(\gamma a)\right] b_n = 0. \tag{22}$$

The system may be rewritten in matrix form $\mathbf{Z_n}\overline{C}_n = \overline{0}$. Here

$$\overline{C}_n = \begin{bmatrix} a_n \\ b_n \end{bmatrix}. \tag{23}$$

I find the eigenvalues by sweeping over the axial wavenumber β to find the zeros of the determinant of the system matrix $\mathbf{Z_n}$

$$\left[\gamma^2\mathrm{J}_n(\gamma a) + \imath Z\omega\epsilon\gamma\mathrm{J}'_n(\gamma a)\right]\left[\imath\omega\mu\gamma\mathrm{J}'_n(\gamma a) + Z\gamma^2\mathrm{J}_n(\gamma a)\right] + Z\beta^2n^2/a^2\mathrm{J}_n^2(\gamma a) = 0. \tag{24}$$

The coefficients a_{nj} and b_{nj} are found from the eigenvectors of $\mathbf{Z_n}$, where the second subscript indexes the eigenvalue β_{nj} associated with eigenvector $\overline{C}_{nj}$.

Each mode was subsequently normalized by ensuring the following orthogonality condition was satisfied

$$\int_0^{2\pi}\int_0^a \hat{\overline{z}}\cdot\overline{E}_p\times\overline{H}_q^*\rho d\rho d\phi = \begin{cases}\delta_{pq}, & \Im\{\beta_{p,q}\}=0\\ -\imath\delta_{pq}, & \Im\{\beta_{p,q}\}>0\end{cases} \tag{25}$$

where $\overline{E}_p$ is the electric field due to the waveguide mode mi, $\overline{H}_q$ the magnetic field due waveguide mode nj, and $\beta_{p,q}$ are the eigenvalues for modes p and q, respectively. The first case where $\Im\{\beta_{p,q}\}=0$ corresponds to propagating modes. Such modes carry real power in the direction of propagation. The condition $\Im\{\beta_{p,q}\}>0$ identifies modes that evanesce in the z-direction. Evanescent modes carry imaginary power along axis of the waveguide which accounts for the $\imath$ multiplying the delta function in Equation (25). Once (25) is satisfied, the resulting modes form a complete orthonormal basis over the area of the hole.

The evolution of the modes from decoupled TE and TM modes in the case of perfectly conducting walls to hybrid modes in the IBC case is of some interest. Note that when the surface impedance Z is set to zero, Equation (24) reduces to

$$\mathrm{J}_n(\gamma a)\mathrm{J}_n'(\gamma a)=0. \tag{26}$$

Two families of solutions result. The eigenvalues of the TM modes for a PEC guide are obtained from the zeros of the Bessel function, while the eigenvalues of the TE modes may be obtained from the zeros of the first derivative of the Bessel function. Thus Equation (24) may be viewed as a generalization of the characteristic equation for the eigenvalues of a circular PEC waveguide.

The polarization of the incident field, together with symmetry considerations, determines the modes that are excited inside the hole. The azimuthal symmetry of the hole dictates that the overlap integrals between the incident field and the hybrid modes vanish for azimuthal numbers other than $n=1$ or $n=-1$. Therefore, there is a strong coupling between the doubly-degenerate $n=1$ mode and the incident plane wave.

4. EIGENFUNCTION EXPANSIONS

4.1. Incident Field

The excitation is a plane wave of arbitrary angle and frequency incident from region 1. Define the following rotation matrices:

$$\mathbf{R}^{(\phi_0)}=\begin{bmatrix}\cos(\phi_0) & \sin(\phi_0) & 0\\ -\sin(\phi_0) & \cos(\phi_0) & 0\\ 0 & 0 & 1\end{bmatrix} \tag{27}$$

and

$$\mathbf{R}^{(\theta_0)}=\begin{bmatrix}1 & 0 & 0\\ 0 & \cos(\theta_0) & \sin(\theta_0)\\ 0 & -\sin(\theta_0) & \cos(\theta_0)\end{bmatrix} \tag{28}$$

along with the vectors

$$\overline{k}^{(0)}=\begin{bmatrix}k_x^0\\ k_y^0\\ k_z^0\end{bmatrix} \tag{29}$$

and

$$\overline{P}^{(0)}=\begin{bmatrix}\cos(\alpha_0)\\ \sin(\alpha_0)\\ 0\end{bmatrix}. \tag{30}$$

Here the incident propagation direction vector $\overline{k}^{(0)}$ is defined by

$$\overline{k}^{(0)}=-\begin{bmatrix}\sin(\theta_0)\cos(\phi_0)\\ \sin(\theta_0)\sin(\phi_0)\\ \cos(\theta_0)\end{bmatrix}. \tag{31}$$

The incident electric and magnetic fields are given by $\overline{E}^{(0)}=\mathbf{R}^{(\theta_0)}\mathbf{R}^{(\phi_0)}\overline{P}^{(0)}$ and $\overline{H}^{(0)}=k\overline{k}^{(0)}\times\overline{E}^{(0)}/(\omega\mu_0)$.

4.2. Regions 1 and 3

Above and below the film, the fields are expanded in terms of TM and TE Floquet modes:

$$\psi_{mn}^{(1,3)}(x,y,z) = A_{mn}^{(1,3)} \exp\left[\imath \overline{k}_{mn} \cdot \boldsymbol{\rho} \pm \imath \beta_{mn}(z \mp t/2)\right] / \sqrt{D_x D_y} \tag{32}$$

and

$$\varphi_{mn}^{(1,3)}(x,y,z) = B_{mn}^{(1,3)} \exp\left[\imath \overline{k}_{mn} \cdot \boldsymbol{\rho} \pm \imath \beta_{mn}(z \mp t/2)\right] / \sqrt{D_x D_y} \tag{33}$$

where $\overline{k}_{mn} = 2\pi(m\hat{\overline{x}}/D_x + n\hat{\overline{y}}/D_y)$, $\boldsymbol{\rho} = x\hat{\overline{x}} + y\hat{\overline{y}}$, $\beta_{mn}^2 = k^2 - (2\pi m/D_x)^2 - (2\pi n/D_y)^2$, and $A_{mn}^{(1,3)}$ and $B_{mn}^{(1,3)}$ are unknown coefficients. The transverse electric and magnetic fields associated with each mode are given by

$$\overline{E}_{tmn}^{(1,3)\prime}(x,y,z) = \mp\left(\beta_{mn} k_x \hat{\overline{x}} + \beta_{mn} k_y \hat{\overline{y}}\right) \psi_{mn}^{(1,3)}(x,y,z), \tag{34}$$

$$\overline{H}_{tmn}^{(1,3)\prime}(x,y,z) = \left(\omega\epsilon k_y \hat{\overline{x}} - \omega\epsilon k_x \hat{\overline{y}}\right) \psi_{mn}^{(1,3)}(x,y,z), \tag{35}$$

$$\overline{E}_{tmn}^{(1,3)\prime\prime}(x,y,z) = \left(-\omega\mu k_y \hat{\overline{x}} + \omega\mu k_x \hat{\overline{y}}\right) \varphi_{mn}^{(1,3)}(x,y,z), \tag{36}$$

and

$$\overline{H}_{tmn}^{(1,3)\prime\prime}(x,y,z) = \mp\left(\beta_{mn} k_x \hat{\overline{x}} + \beta_{mn} k_y \hat{\overline{y}}\right) \varphi_{mn}^{(1,3)}(x,y,z) \tag{37}$$

where $k_x = 2\pi m/D_x$ and $k_y = 2\pi n/D_y$. When $m = n = 0$, two additional modes are necessary to span the space

$$\begin{aligned} \overline{E}^{(1,3)\prime}(z) &= A_{00}^{(1,3)} \exp[\pm\imath k(z \mp t/2)]\hat{\overline{x}} \\ \overline{H}^{(1,3)\prime}(z) &= \pm k/(\omega\mu) A_{00}^{(1,3)} \exp[\pm\imath k(z \mp t/2)]\hat{\overline{y}} \end{aligned} \tag{38}$$

and

$$\begin{aligned} \overline{E}^{(1,3)\prime\prime}(z) &= B_{00}^{(1,3)} \exp[\pm\imath k(z \mp t/2)]\hat{\overline{y}} \\ \overline{H}^{(1,3)\prime\prime}(z) &= \mp k/(\omega\mu) B_{00}^{(1,3)} \exp[\pm\imath k(z \mp t/2)]\hat{\overline{x}}. \end{aligned} \tag{39}$$

4.3. Region 2

Inside the hole, I expand the fields in a series consisting of the waveguide modes defined in Section 3. The transverse components of the total field inside the hole are therefore

$$\overline{E}_t^{(2)}(\rho,\phi,z) = \sum_{nj} \left[C_{nj} \exp(\imath\beta_{nj} z) + D_{nj} \exp(-\imath\beta_{nj} z)\right] \left[E_{\rho nj}(\rho)\hat{\boldsymbol{\rho}} + E_{\phi nj}(\rho)\hat{\boldsymbol{\phi}}\right] \exp(\imath n\phi) \tag{40}$$

and

$$\overline{H}_t^{(2)}(\rho,\phi,z) = \sum_{nj} \left[C_{nj} \exp(\imath\beta_{nj} z) - D_{nj} \exp(-\imath\beta_{nj} z)\right] \left[H_{\rho nj}(\rho)\hat{\boldsymbol{\rho}} + H_{\phi nj}(\rho)\hat{\boldsymbol{\phi}}\right] \exp(\imath n\phi) \tag{41}$$

where

$$E_{\rho nj}(\rho) = \imath\beta_{nj}\gamma_{nj} \mathrm{J}_n'(\gamma_{nj}\rho) a_{nj} - \omega\mu n \mathrm{J}_n(\gamma_{nj}\rho)/\rho b_{nj} \tag{42}$$

$$E_{\phi nj}(\rho) = -n\beta_{nj} \mathrm{J}_n(\gamma_{nj}\rho)/\rho a_{nj} - \imath\omega\mu\gamma_{nj} \mathrm{J}_n'(\gamma_{nj}\rho) b_{nj} \tag{43}$$

$$H_{\rho nj}(\rho) = \omega\epsilon n \mathrm{J}_n(\gamma_{nj}\rho)/\rho a_{nj} + \imath\beta_{nj}\gamma_{nj} \mathrm{J}_n'(\gamma_{nj}\rho) b_{nj} \tag{44}$$

$$H_{\phi nj}(\rho) = \imath\omega\epsilon\gamma_{nj} \mathrm{J}_n'(\gamma_{nj}\rho) a_{nj} - \beta_{nj} n \mathrm{J}_n(\gamma_{nj}\rho)/\rho b_{nj} \tag{45}$$

and C_{nj} and D_{nj} are unknown waveguide mode coefficients.

5. MATRIX EQUATIONS

I enforce an impedance boundary condition on the metal-air interfaces and continuity of the tangential electric field over the hole area at $z = \pm t/2$:

$$\overline{E}_t^{(1,3)} = \begin{cases} \pm Z\hat{\overline{z}} \times \overline{H}^{(1,3)}, & \rho \geq a \\ \overline{E}_t^{(2)}(\pm t/2), & \rho < a. \end{cases} \tag{46}$$

Testing (46) with the appropriate TM or TE mode leads to the following matrix equations

$$\mathbf{Z}^{(e1)}\overline{A} + \overline{V}^{(e0)} = \mathbf{M}^{(e1)}\left[\mathbf{D}^{(1)}\overline{C}^{(+)} + \mathbf{D}^{(2)}\overline{C}^{(-)}\right] \tag{47}$$

and

$$\mathbf{Z}^{(e2)}\overline{B} = \mathbf{M}^{(e2)}\left[\mathbf{D}^{(2)}\overline{C}^{(+)} + \mathbf{D}^{(1)}\overline{C}^{(-)}\right]. \tag{48}$$

The matrices

$$Z_{uv}^{(e1)} = \int_U \overline{H}_u \cdot \overline{E}_v^{(1)} dxdy - Z\int_S \overline{H}_u \cdot \hat{\overline{z}} \times \overline{H}_v^{(1)} dxdy \tag{49}$$

and

$$M_{uv}^{(e1)} = \int_H \overline{H}_u \cdot \overline{E}_v^{(2)} \rho d\rho d\phi \tag{50}$$

contain the overlap integrals between testing $\overline{H}_u = \hat{\overline{z}} \times \overline{H}_{tmn}^*$ and basis functions $\overline{E}_v^{(1,3)} = \overline{E}_{tpq}^{(1,3)}$ and $\overline{H}_v^{(1,3)} = \overline{H}_{tpq}^{(1,3)}$. Here $\overline{E}_v^{(2)} = E_{\rho nj}(\rho)\hat{\boldsymbol{\rho}} + E_{\phi nj}(\rho)\hat{\boldsymbol{\phi}}$ is the electric field associated with a waveguide mode, U the area of the unit cell, S the area covered by the metal, and H the area of the hole. The integrals over the azimuthal direction were calculated analytically while the remaining integral over the radial direction was computed by quadrature. The matrices $D_{vv}^{(1,2)} = \exp(\pm\imath\beta_{nj}t/2)$ contain phase terms for each waveguide mode. The overlap integrals between regions 2 and 3 are included in

$$Z_{uv}^{(e2)} = \int_U \overline{H}_u \cdot \overline{E}_v^{(3)} dxdy - Z\int_S \overline{H}_u \cdot \hat{\overline{z}} \times \overline{H}_v^{(3)} dxdy \tag{51}$$

and

$$M_{uv}^{(e2)} = \int_H \overline{H}_u \cdot \overline{E}_v^{(2)} \rho d\rho d\phi. \tag{52}$$

The overlap between testing functions and the incident field is contained in the vector

$$V_u^{(e0)} = \int_U \overline{H}_u \cdot \overline{E}^{(0)} dxdy - Z\int_S \overline{H}_u \cdot \hat{\overline{z}} \times \overline{H}^{(0)} dxdy. \tag{53}$$

The vector $\overline{A}$ contains the unknowns from region 1, and $\overline{B}$ contains the unknowns from region 3. $C_v^{(+)} = C_{nj}$ and $C_v^{(-)} = D_{nj}$ are the unknown waveguide mode amplitudes.

Continuity of the tangential components of the magnetic field is enforced over the hole area only

$$\overline{H}_t^{(1,3)} = \overline{H}_t^{(2)}(\pm t/2), \quad \rho < a. \tag{54}$$

Testing the magnetic field with waveguide modes leads to the following matrix equations:

$$\mathbf{M}^{(h1)}\overline{A} + \overline{V}^{(h0)} = \mathbf{D}^{(1)}\overline{C}^{(+)} - \mathbf{D}^{(2)}\overline{C}^{(-)} \tag{55}$$

$$\mathbf{M}^{(h2)}\overline{B} = \mathbf{D}^{(2)}\overline{C}^{(+)} - \mathbf{D}^{(1)}\overline{C}^{(-)} \tag{56}$$

where

$$M_{uv}^{(h1)} = \int_H \overline{E}_u \cdot \overline{H}_v^{(1)} \rho d\rho d\phi \tag{57}$$

and

$$M_{uv}^{(h2)} = \int_H \overline{E}_u \cdot \overline{H}_v^{(3)} \rho d\rho d\phi \tag{58}$$

contain the overlap integrals between regions 1 and 2 and 2 and 3, respectively. Here I test with the electric field of a waveguide mode given by $\overline{E}_u = -\hat{\overline{z}} \times [E^*_{\rho mi}(\rho)\hat{\boldsymbol{\rho}} + E^*_{\phi mi}(\rho)\hat{\boldsymbol{\phi}}]$. The basis functions in region 1 and 3 are given by $\overline{H}_v^{(1,3)} = \overline{H}_{tpq}^{(1,3)}$. Once again, the overlap between testing functions and the incident field is contained in the vector

$$V_u^{(h0)} = \int_H \overline{E}_u \cdot \overline{H}^{(0)} \rho d\rho d\phi. \tag{59}$$

It remains to solve for the unknown coefficients contained in $\overline{A}$ and $\overline{B}$. I begin by solving for the waveguide mode coefficient vectors $\overline{C}^{(+)}$ and $\overline{C}^{(-)}$:

$$\overline{C}^{(+)} = \mathbf{M}^{(f)-1}\left[\overline{S}^{(e0)} + \overline{S}^{(h0)}\right] \tag{60}$$

$$\overline{C}^{(-)} = -\mathbf{Q}^{(mr)-1}\mathbf{Q}^{(pr)}\overline{C}^{(+)}. \tag{61}$$

The intermediate quantities are defined in the Appendix. The unknown vectors $\overline{A}$ and $\overline{B}$ are determined from $\overline{C}^{(+)}$ and $\overline{C}^{(-)}$:

$$\overline{A} = \mathbf{Z}^{(e1)-1}\left[-\overline{V}^{(e0)} + \mathbf{M}^{(e1)}\mathbf{D}^{(1)}\overline{C}^{(+)} + \mathbf{M}^{(e1)}\mathbf{D}^{(2)}\overline{C}^{(-)}\right] \tag{62}$$

$$\overline{B} = \mathbf{Z}^{(e2)-1}\left[\mathbf{M}^{(e2)}\mathbf{D}^{(2)}\overline{C}^{(+)} + \mathbf{M}^{(e2)}\mathbf{D}^{(1)}\overline{C}^{(-)}\right]. \tag{63}$$

Once $\overline{B}$ is known, the transmission through the film may be calculated.

6. RESULTS

Consider transmission through a 320 nm thick silver film perforated by a square array of circular holes of radius 140 nm and lattice constant 750 nm at normal incidence (Figure 2). The transmission-to-area efficiency is defined as the ratio between the energy transmitted through the film to the area of the film covered by the holes. The holes cover only 11% of the area of the film, yet the peak transmission is nearly 15%, a transmission-to-area efficiency of roughly 130%. Martin-Moreno and Garcia-Vidal further point out that single aperture theory (which assumes a PEC screen) predicts a transmission efficiency on the order of 1% in this frequency regime. The much larger transmission through the perforated film relative to that predicted by single aperture theory explains the descriptor "extraordinary" in the name

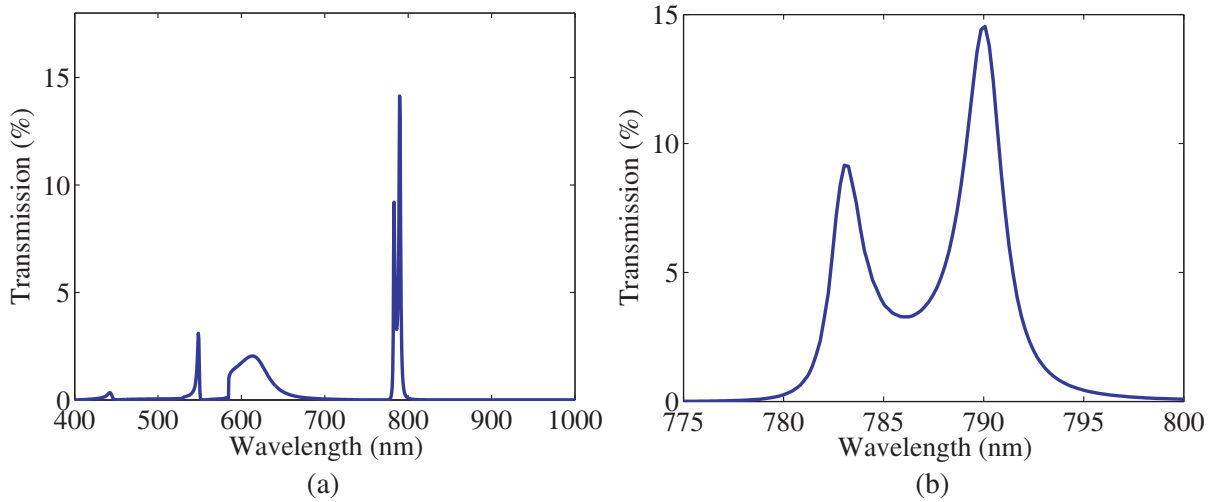

Figure 2. (Color online) Theoretical extraordinary transmission through a 320 nm thick silver film perforated by an array of circular holes of radius 140 nm and lattice constant 750 nm at normal incidence (a) from 400 to 1000 nm and (b) from 775 to 800 nm.

of the phenomenon. Note also the presence of the null in the transmission profile at a wavelength of 750 nm associated with Wood's anomaly.

The theory presented here agrees well with the experimental peak transmission through a finite array of 21×21 circular holes ([34], Figure 1). The method herein predicts the amplitude of the first-order SPP transmission peak to within a relative error of $\pm 15\%$ of the experimental value. Previous modal approaches significantly over-estimate the transmission around a wavelength of 800 nm, ranging from 43% [29] if an IBC is imposed on the upper and lower horizonatal surfaces only to 50% [34] for an infinite PEC array. Small variations in the finite array hole diameters may explain the broader peaks in the experimental data. However, the overestimation of peak transmission is related to the boundary condition on the hole wall.

The improved agreement between experiment and theory when an IBC is included in the hole may be attributed to a more realistic model of the fundamental mode. For sufficiently subwavelength apertures at optical wavelengths, the fundamental mode dominates the fields inside the hole. When an IBC is imposed on the hole wall, the fundamental is the hybrid HEM11 mode (Figures 3 and 4). Here the azimuthal number is one and I take the first eigenvalue. Both TM and TE potentials contribute to the fundamental under the IBC approximation. Notice that a significant tangential electric field exists on the surface of the hole at $\rho = a$ (Figures 3(a), (b) and 4(a), (b)). If the IBC is replaced with a PEC as in [29] and [34], the fields are squeezed to allow a null on the hole wall (Figures 3(c), (d) and 4(c), (d)). In order to compensate for this, Martin-Moreno and Garcia-Vidal enlarge the hole by assuming an effective hole radius equal to the original value plus twice the skin depth [29]. Enlarging the hole extends the field past the true hole radius and neglects losses in the silver. Energy that should be absorbed leaks through and the transmission is overestimated.

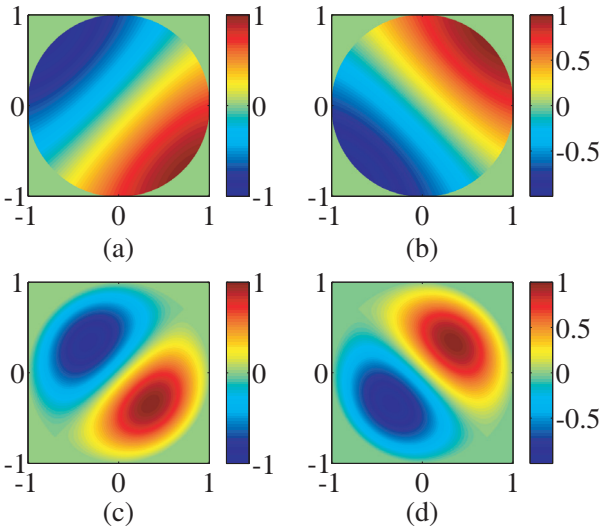

Figure 3. (Color online) Normalized z-component of the electric field for the fundamental mode at a wavelength of 790 nm. The x and y-axes have been normalized by the hole radius. The panels show the (a) real and (b) imaginary parts of the field for the fundamental hybrid HEM11 mode used with an IBC on the hole wall. The remaining panels show the (c) real and (d) imaginary parts of the field for the fundamental TE11 mode used with a PEC boundary condition on the hole wall.

Next I study the impact of film thickness, hole radius, and lattice constant on the transmission profile for the purpose of identifying a mechanism for EOT. Surface plasmon polaritons tied to the interface between a dielectric and a metal have been included in a possible mechanism [34, 35]. While the exact role of surface waves in EOT has been a matter of debate, they help to explain the results reported herein. First, note that transmission through the film is a strong function of the film thickness (Figure 5). The transmission peaks are associated with waves bound to the top and bottom surfaces. When the film is thin, coupling between the upper and lower surfaces is strong and two peaks at different wavelengths may be observed. As the film thickness increases, the coupling weakens and the

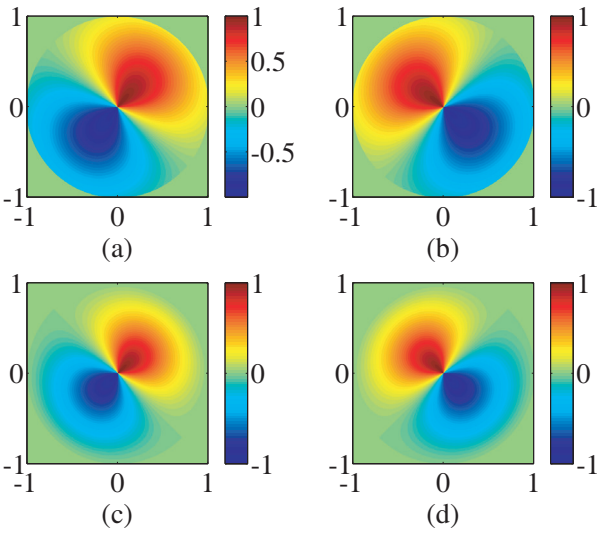

Figure 4. (Color online) Normalized ϕ-component of the electric field for the fundamental mode at a wavelength of 790 nm. The x and y-axes have been normalized by the hole radius. The panels show the (a) real and (b) imaginary parts of the field for the fundamental hybrid HEM11 mode used with an IBC on the hole wall. The remaining panels show the (c) real and (d) imaginary parts of the field for the fundamental TE11 mode used with a PEC boundary condition on the hole wall.

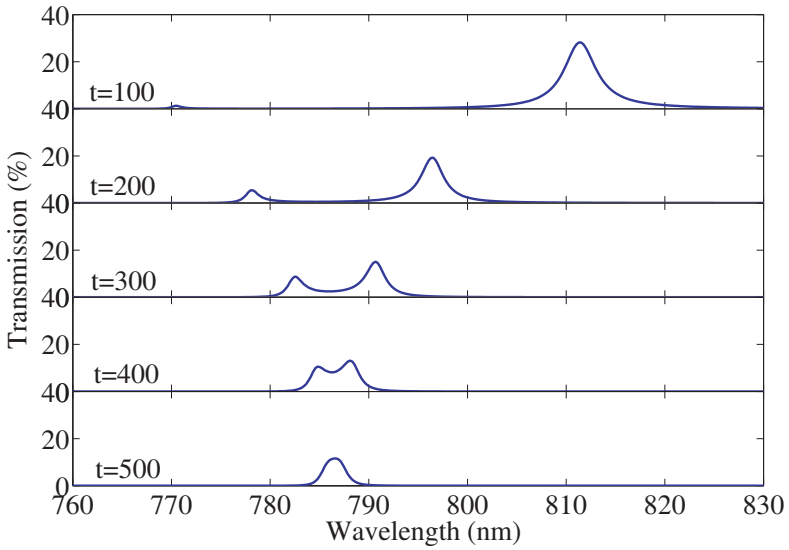

Figure 5. (Color online) Theoretical transmission for the film thicknesses listed in the panel.

peaks merge. The response for the 500 nm thick film is dominated by uncoupled surfaces waves.

Both the amplitude and position of the the transmission peaks are affected by the hole radius (Figure 6). Unsurprisingly, larger holes transmit more energy through the film. The peaks also shift towards longer wavelengths as the radius of the hole increases. This wavelength shift is related to the resonant character of the transmission process. The peaks occur for holes of a certain size relative to the wavelength. As the wavelength increases, this relative size remains roughly constant. The peak position increases to maintain the resonant ratio between hole radius and wavelength.

The lattice constant also significantly affects the transmission profile (Figure 7). The peaks consistently occur at a wavelength slightly greater than the lattice constant. The amplitude of the transmission peaks decreases as the lattice constant increases. For a constant hole radius, a smaller

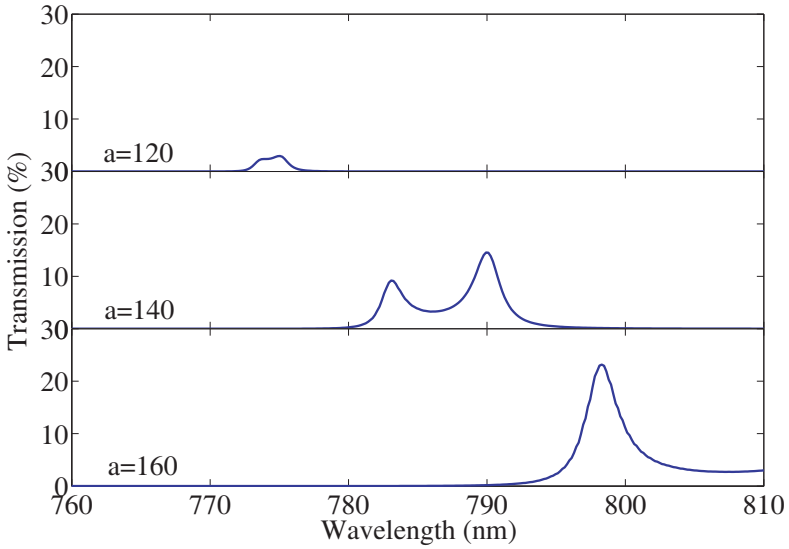

Figure 6. (Color online) Theoretical transmission for the hole radii listed in the panel for a 320 nm thick film with lattice constant 750 nm.

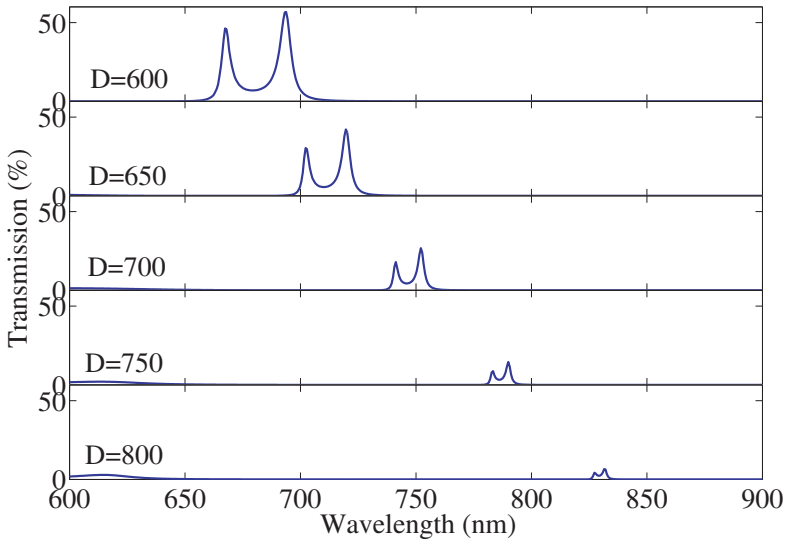

Figure 7. (Color online) Theoretical transmission for the lattice constants listed in the panel for a 320 nm thick film with hole radius of 140 nm.

fraction of the film area is covered by the holes as the lattice constant increases and less energy is transmitted. However, the transmission-to-area efficiency is not constant with respect to lattice constant (Figure 8). For a lattice constant $D = 600$ nm, 17% of the film area is covered by the holes. I observe a maximum transmission of approximately 57% for a transmission-to-area efficiency of roughy 335%. The efficiency decreases to 68% for a lattice constant of 800 nm. Smaller lattice constants appear to be more efficient than larger lattice constants. Surface waves again help to explain this trend. Martin-Moreno et al. identify modes supported by a single interface with parallel momentum $2\pi/D$, the so-called first-order surface plasmon polariton [34]. As the lattice constant decreases, more parallel momentum is carried by the first-order SPP. The surface wave traps more energy that is funneled through the film by the fundamental mode.

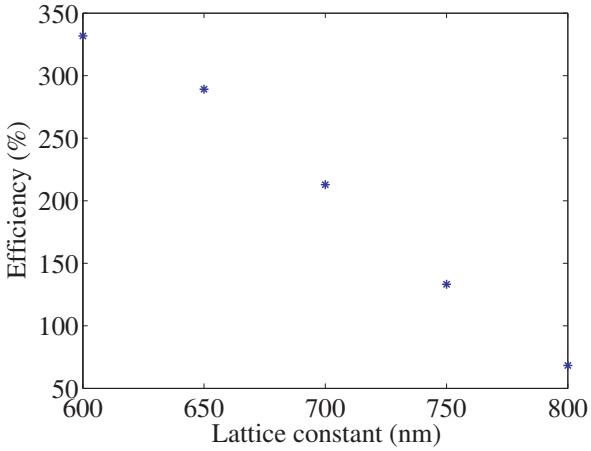

Figure 8. (Color online) Theoretical transmission-to-area efficiency as a function of lattice constant.

7. CONCLUSIONS

A mode-matching solution to plane wave scattering by a silver film perforated by an infinite array of circular holes has been presented. Impedance boundary conditions have been imposed on all surfaces. While the approach detailed herein is quite general, it has a few limitations. As the hybrid modes form a complete orthogonal basis set over the hole region, they are sufficient to represent the fields inside a hole of arbitrary radius. However, the larger the hole with respect to wavelength the more modes are necessary to accurately represent the field. The method is valid in wavelength regimes where the impedance boundary condition remains an accurate approximation. The results predict a peak transmission value that is in good agreement with experiment. Extraordinary optical transmission has been studied as a function of film thickness, hole radius, lattice constant, and angle of incidence. The transmission profile position, shape, and amplitude are strong functions of film thickness, hole radius, and lattice constant. The coupling between modes bound to the upper and lower surfaces is strongly affected by film thickness. The resonant nature of the EOT process dictates that transmission peaks occur for holes of a roughly constant electrical size. Small lattice constants transmit energy more efficiently than larger ones for the film under study. The results support the inclusion of surface waves in the mechanism for EOT.

APPENDIX A. INTERMEDIATE MATRIX DEFINITIONS

$$\mathbf{P}^{(p)} = \mathbf{M}^{(h1)}\mathbf{Z}^{(e1)-1}\mathbf{M}^{(e1)}\mathbf{D}^{(1)} - \mathbf{D}^{(1)} \tag{A1}$$

$$\mathbf{P}^{(m)} = \mathbf{M}^{(h1)}\mathbf{Z}^{(e1)-1}\mathbf{M}^{(e1)}\mathbf{D}^{(2)} + \mathbf{D}^{(2)} \tag{A2}$$

$$\overline{R}^{(e0)} = \mathbf{M}^{(h1)}\mathbf{Z}^{(e1)-1}\overline{V}^{(e0)} \tag{A3}$$

$$\overline{R}^{(h0)} = \overline{V}^{(h0)} \tag{A4}$$

$$\mathbf{Q}^{(p)} = \mathbf{M}^{(h2)}\mathbf{Z}^{(e2)-1}\mathbf{M}^{(e2)}\mathbf{D}^{(2)} - \mathbf{D}^{(2)} \tag{A5}$$

$$\mathbf{Q}^{(m)} = \mathbf{M}^{(h2)}\mathbf{Z}^{(e2)-1}\mathbf{M}^{(e2)}\mathbf{D}^{(1)} + \mathbf{D}^{(1)} \tag{A6}$$

The dimension of these matrices is N, the number of Floquet modes used in the series. Often more modes are needed to represent the fields above and below the film than inside the hole. This results in nonsquare matrices upon testing. In order to solve the system, I reduce the dimensionality of the larger matrices:

$$\mathbf{P}^{(pr)} = \mathbf{P}^{(p)}_{1:N_h,1:N_h} \tag{A7}$$

$$\mathbf{P}^{(mr)} = \mathbf{P}^{(m)}_{1:N_h,1:N_h} \tag{A8}$$

$$\mathbf{Q}^{(pr)} = \mathbf{Q}^{(p)}_{1:N_h,1:N_h} \tag{A9}$$

$$\mathbf{Q}^{(mr)} = \mathbf{Q}^{(m)}_{1:N_h,1:N_h}. \tag{A10}$$

Here N_h is the number of waveguide modes in the hole region.

$$\mathbf{M}^{(f)} = \mathbf{Q}^{(pr)} - \mathbf{Q}^{(mr)}\mathbf{P}^{(mr)-1}\mathbf{P}^{(pr)} \tag{A11}$$

$$\overline{S}^{(e0)} = -\mathbf{Q}^{(mr)}\mathbf{P}^{(mr)-1}\overline{R}^{(e0)} \tag{A12}$$

$$\overline{S}^{(h0)} = \mathbf{Q}^{(mr)}\mathbf{P}^{(mr)-1}\overline{R}^{(h0)} \tag{A13}$$

REFERENCES

1. Pendry, J. B., "Playing tricks with light," *Science*, Vol. 285, 1687, 1999.
2. Politano, A., "Influence of structural and electronic properties on the collective excitations of Ag/Cu(111)," *Plasmonics*, Vol. 7, No. 1, 131–136, 2012.
3. Politano, A., "Low-energy collective electronic mode at a noble metal interface," *Plasmonics*, Vol. 8, No. 2, 357–360, 2013.
4. Politano, A., V. Formoso, and G. Chiarello, "Dispersion and damping of gold surface plasmon," *Plasmonics*, Vol. 3, No. 4, 165, 2008.
5. Politano, A., V. Formoso, and G. Chiarello, "Collective electronic excitations in thin Ag films on Ni(111)," *Plasmonics*, Vol. 8, No. 4, 1683–1690, 2013.
6. King, M. D., S. Khadka, G. A. Craig, and M. D. Mason, "Effect of local heating on the SERS efficiency of optically trapped prismatic nanoparticles," *The Journal of Physical Chemistry C*, Vol. 112, No. 31, 11751–11757, 2008.
7. Politano, A. and G. Chiarello, "The influence of electron confinement, quantum size effects, and film morphology on the dispersion and the damping of plasmonic modes in Ag and Au thin films," *Prog. Surf. Sci.*, Vol. 90, No. 2, 144–193, 2015.
8. Haynes, C. L., A. D. McFarland, and R. P. Van Duyne, "Surface-enhanced raman spectroscopy," *Anal. Chem.*, Vol. 77, No. 17, 338A–346A, 2005.
9. Politano, A., A. Cupolillo, G. Di Profio, H. A. Arafat, G. Chiarello, and E. Curcio, "When plasmonics meets membrane technology," *Journal of Physics: Condensed Matter*, Vol. 28, No. 36, 363003, 2016.
10. Politano, A., P. Argurio, G. Di Profio, V. Sanna, A. Cupolillo, S. Chakraborty, H. A. Arafat, and E. Curcio, "Photothermal membrane distillation for seawater desalination," *Advanced Materials*, Vol. 29, No. 2, 1603504, 2017.
11. Harmsen, S., R. Huang, M. A. Wall, H. Karabeber, J. M. Samii, M. Spaliviero, J. R. White, S. Monette, R. O'Connor, K. L. Pitter, S. A. Sastra, M. Saborowski, E. C. Holland, S. Singer, K. P. Olive, S. W. Lowe, R. G. Blasberg, and M. F. Kircher, "Surface-enhanced resonance Raman scattering nanostars for high-precision cancer imaging," *Science Translational Medicine*, Vol. 7, No. 271, 271ra7–271ra7, 2015.
12. Krenn, J. R., A. Dereux, J. C. Weeber, E. Bourillot, Y. Lacroute, J. P. Goudonnet, G. Schider, W. Gotschy, A. Leitner, F. R. Aussenegg, and C. Girard, "Squeezing the optical near-field zone by plasmon coupling of metallic nanoparticles," *Phys. Rev. Lett.*, Vol. 82, 2590, 1999.
13. Krenn, J. R., B. Lamprecht, H. Ditlbacher, G. Schider, M. Salerno, A. Leitner, and F. R. Aussenegg, "Non-diffraction limited light transport by gold nanowires," *Europhys. Lett.*, Vol. 60, No. 5, 663–669, 2001.
14. Lamprecht, B., J. R. Krenn, G. Schider, H. Ditlbacher, M. Salerno, N. Felidj, A. Leitner, F. R. Aussenegg, and J. C. Weeber, "Surface plasmon propagation in microscale metal stripes," *Appl. Phys. Lett.*, Vol. 79, No. 1, 513, 2001.
15. Maier, S. A., P. G. Kik, H. A. Atwater, S. Meltzer, E. Harel, B. E. Koel, and A. A. Requicha, "Local detection of electromagnetic energy transport below the diffraction limit in metal nanoparticle plasmon waveguides," *Nature Materials*, Vol. 2, 229–232, 2003.

16. Zia, R., M. D. Selker, P. B. Catrysse, and M. L. Brongersma, "Geometries and materials for subwavelength surface plasmon modes," *J. Opt. Soc. Am. A*, Vol. 21, No. 12, 2442, 2005.
17. De Menezes, J. W., A. Thesing, C. Valsecchi, L. E. G. Armas, and A. G. Brolo, "Improving the performance of gold nanohole array biosensors by controlling the optical collimation conditions," *Appl. Opt.*, Vol. 54, No. 21, 6502–6507, 2015.
18. Li, X., M. Soler, C. I. Ozdemir, A. Belushkin, F. Yesilkoy, and H. Altug, "Plasmonic nanohole array biosensor for label-free and real-time analysis of live cell secretion," *Lab Chip*, Vol. 17, No. 13, 2017.
19. Cetin, A. E., D. Etezadi, B. C. Galarreta, M. P. Busson, Y. Eksioglu, and H. Altug, "Plasmonic nanohole arrays on a robust hybrid substrate for highly sensitive label-free biosensing," *ACS Photonics*, Vol. 2, No. 8, 1167–1174, 2015.
20. Ebbesen, T. W., H. J. Lezec, H. F. Ghaemi, T. Thio, and P. A. Wolff, "Extraordinary optical transmission through sub-wavelength hole arrays," *Nature*, Vol. 391, 667–669, 1998.
21. Bethe, H. A., "Theory of diffraction by small holes," *Phys. Rev.*, Vol. 66, 163, 1944.
22. Baida, F. I. and D. Van Labeke, "Three-dimensional structures for enhanced transmission through a metallic film: Annular aperture arrays," *Phys. Rev. B*, Vol. 67, 155314, 2003.
23. Li, Z. and L. Lin, "Photonic band structures solved by a plane-wave-based transfer-matrix method," *Phys. Rev. E*, Vol. 67, 046607, 2003.
24. Biswas, R., C. G. Ding, I. Puscasu, M. Pralle, M. McNeal, J. Daly, A. Greenwald, and E. Johnson, "Theory of subwavelength hole arrays coupled with photonic crystals for extraordinary thermal emission," *Phys. Rev. B*, Vol. 74, 045106, 2006.
25. Martin-Moreno, L. and F. J. Garcia-Vidal, "Minimal model for optical transmission through holey metal films," *J. Phys.: Condens. Matter*, Vol. 20, 304214, 2008.
26. De Leon-Perez, F., G. Brucoli, F. J. Garcia-Vidal, and L. Martin-Moreno, "Theory on the scattering of light and surface plasmon polaritons by arrays of holes and dimples in a metal film," *New Journal of Physics*, Vol. 10, 105017, 2008.
27. Zhang, M., C. Huang, G. Huang, and Y. Zhu, "Theory of extraordinary light transmission through sub-wavelength circular hole arrays," *Journal of Optics*, Vol. 12, 015004, 2010.
28. Huang, C., Q. Wang, and Y. Zhu, "Dual effect of surface plasmons in light transmission through perforated metal films," *Physical Review B*, Vol. 75, 245421, 2007.
29. Martin-Moreno, L. and F. J. Garcia-Vidal, "Optical transmission through circular hole arrays in optically thick metal films," *Optics Express*, Vol. 12, 3619, 2004.
30. Rothwell, E. J. and M. J. Cloud, *Electromagnetics*, CRC Press LLC, Boca Raton, FL, 2001.
31. Tretyakov, S., *Analytical Modeling in Applied Electromagnetics*, Artech House, Inc., Norwood, MA, 2003.
32. Hunter, J. K. and B. Nachtergaele, *Applied Analysis*, World Scientific, Hackensack, NJ, 2001.
33. Drude, P., "Zur Elektronentheorie der Metalle," *Ann. Phys.*, Vol. 306, 566–613, 1900.
34. Martin-Moreno, L., F. J. Garcia-Vidal, H. J. Lezec, K. M. Pellerin, T. Thio, J. B. Pendry, and T. W. Ebbesen, "Theory of extraordinary optical transmission through subwavelength hole arrays," *Phys. Rev. Lett.*, Vol. 86, 1114–1117, 2001.
35. Martin-Moreno, L., F. J. Garcia-Vidal, H. J. Lezec, A. Degiron, and T. W. Ebbesen, "Theory of highly directional emission from a single subwavelength aperture surrounded by surface corrugations," *Phys. Rev. Lett.*, Vol. 90, 167401, 2003.